Supplementary information for

"Quantifying the local tissue volume and composition in individual brains with MRI"

Aviv Mezer[1], Jason D. Yeatman[1], Nikola Stikov[2], Kendrick N. Kay[1], Nam–Joon Cho[3,4], Robert F. Dougherty[5], Michael L. Perry[1], Josef Parvizi[6], Le H. Hua[6], Kim Butts-Pauly[7] and Brian Wandell [1, 5]

[1] Department of Psychology, Stanford University, Stanford, CA USA

[2] Montreal Neurological Institute, McGill University, Montreal, Canada

[3] Department of Chemical Engineering, Stanford University, Stanford, CA USA

[4] School of Materials Science and Engineering, Nanyang Technological University, Singapore

[5] Center for Cognitive and Neurobiological Imaging, Stanford University, Stanford University, Stanford, CA USA

[6] Department of Neurology and Neurological Sciences, Stanford University, Stanford, CA USA

[7] Department of Radiology, Stanford University, Stanford, CA USA

Contact: Aviv Mezer avivmezer@gmail.com

Nature Medicine: doi:10.1038/nm.3390

Table of Contents

Supplemental Table 1 - Glossary of terms 3

Supplementary Figure 1- Schematic diagram of the method and tissue model 4

Comparing spoiled-GE and SEIR T1 mapping 5
Supplementary Figure 2 – T1 mapping using SEIR-SS and spoiled-GE 6

Reliability of PD and MTV mapping 7
Supplementary Figure 3 - Proton density measurement with RF-receive correction 8

Reliability of T1 mapping across multiple scans 9
Supplementary Figure 4 - T1 mapping reliability 11
Supplementary Figure 5 - The effect of TR, TE and flip angle on the T1 estimation 12
Supplementary Figure 6 - T1 maps using SEIR-SS and spoiled-GE with RF-excite bias by low spatial frequency bias field correction. 13

Biophysical modeling of T1 and MTV relations 14
T1 modeling approaches slow vs. fast exchange 14
Supplementary Figure 7 - Literature review comparing T1 observed with T1 of water 17
Deriving VIP from T1 and MTV 18
Deriving the compartment characteristic from in-vivo data 19
Supplementary Figure 8- VIP for lipid mixture phantoms 23
Supplementary Figure 9- T1 dependence on field strength predictions 24

MTV Relationship to other quantitative MRI methods 25
Diffusion 25
Quantitative Magnetization Transfer 25
For farther discussion about quantitative magnetization transfer relation to T1 see the above section 'T1 modeling approaches slow vs. fast exchange 'and Supplementary Figure 7. 26
T2 -Myelin Water Fraction 26
Supplementary Figure 10 – The correlation between the mean MTVF and the bound pool fraction (BPF) in white matter tracts 27

Supplementary Figure 11– Tissue abnormalities in individuals with multiple sclerosis 28

Supplementary Figure 12 – T1-weighted and FLAIR axial images in two individuals with multiple sclerosis 29

References 30

Supplemental Table 1 - Glossary of terms

Spoiled-GE	Spoiled Gradient Echo
SEIR	Spin Echo Inversion Recovery
PD	Proton Density
R1	= 1/T1 The longitudinal relaxation rate in units of sec^{-1}
MTV	Macromolecular Tissue Volume
MTVF	Macromolecular Tissue Volume Fraction
WVF	Water Volume Fraction
DI	Dissimilarity Index - between the measured R1 and R1 prediction by MVF
FIWP	Fraction of Interacting Water Protons
VIP	The apparent Volume of Interacting Protons – surface and water
SIR	Surface interaction rate – between macromolecular surface and water

Nature Medicine: doi:10.1038/nm.3390

Supplementary Figure 1- Schematic diagram of the method and tissue model

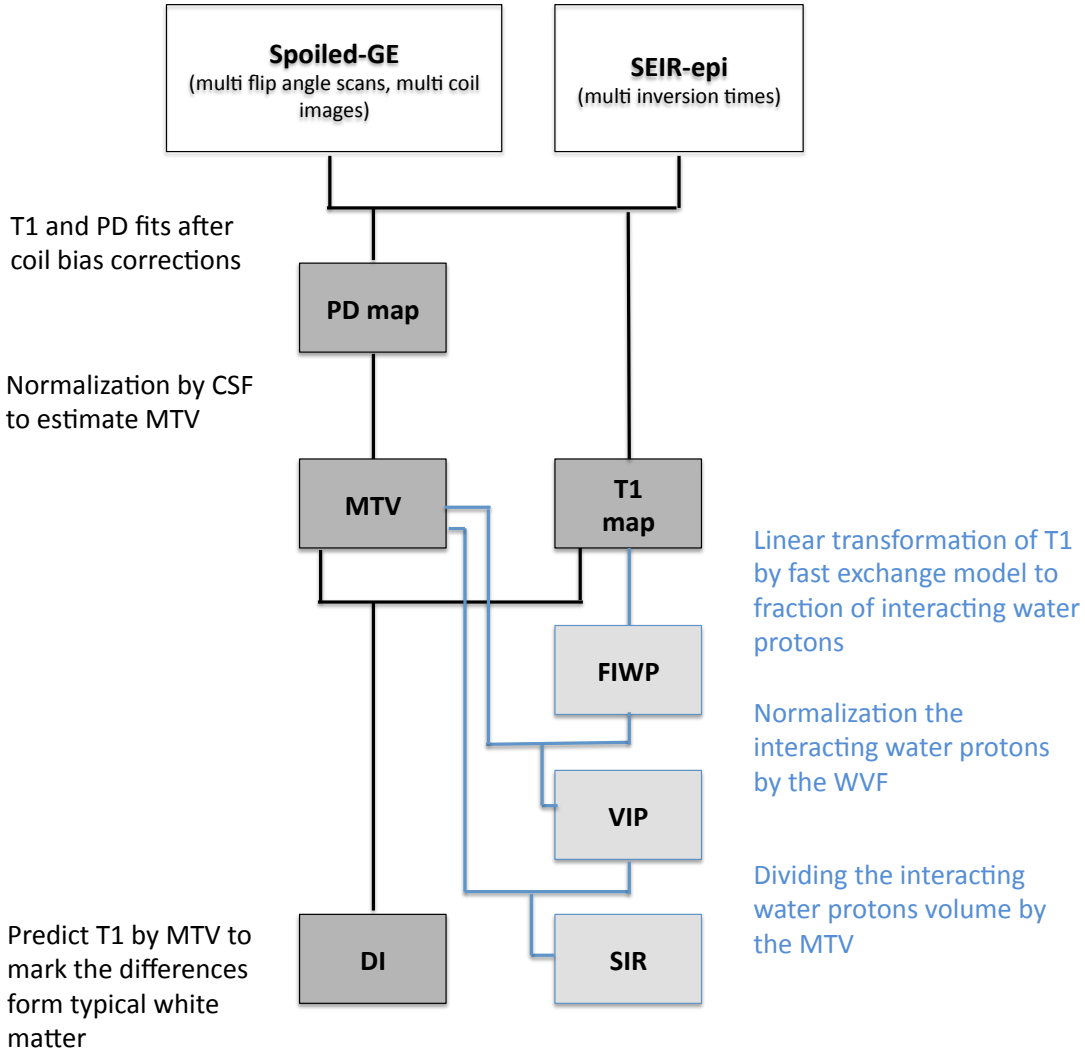

Supplementary Figure 1. Schematic diagram of the method and tissue model. The open boxes describe the data acquisition. The dark gray boxes, black lines and associated text describe the estimation of T1 and PD maps and the derivation of brain tissue properties MTV and DI. The light gray boxes, blue lines, and associated text describe the fast-exchange modeling, starting the T1 and MTV maps and deriving the brain tissue properties, VIP and SIR.

Nature Medicine: doi:10.1038/nm.3390

Comparing spoiled-GE and SEIR T1 mapping

The excite bias inhomogeneities of the spoiled-GE images are removed by using unbiased T1 maps obtained with spin-echo inversion recovery (SEIR) with an echo-planar imaging (EPI) readout. In the Method section we explain how the bias can be calculated from Equation 1.1 as long as the unbiased T1 map is available. The assumption is that that a T1 measure with SEIR-EPI is a good approximation of the single-slice SEIR method (SEIR-SS), which has been suggested as the gold standard for T1 mapping [1]. To test this assumption we compared both phantom and human gold standard SEIR and SEIR-EPI T1 maps. In both cases the T1 agreed well with the coefficient of determination [2] (R^2 =~ 0.91).

Next we evaluated the accuracy of the spoiled-GE T1 estimates at 1.5T and 3T by comparing them to values in the same subject obtained using the SEIR-SS (**Supplementary figure 2**). Panels A and C show final T1 estimates of the spoiled-GE data in 1.5 and 3T after correcting for transmit coil inhomogeneity; panels B and D show the estimates without correcting for transmit coil inhomogeneity. At 3T the coil corrections improve the agreement as measured by the coefficient of determination from R^2=0.14 to R^2=0.66 in the gray and white matter. At 1.5T the coil corrections improve the agreement from R^2=0.44 to R^2=0.58. The root-mean-square error deviation from zero is 11% at 3T and 16% at 1.5T in gray and white matter (excluding CSF). The error varies with the T1 value, as expected [1]. Repeated measures in the gray and white matter, using the SEIR-SS method, have similar reliability. Given the relatively short TR used in this work, repeated measures in the CSF are unreliable.

Nature Medicine: doi:10.1038/nm.3390

Supplementary Figure 2 – T1 mapping using SEIR-SS and spoiled-GE

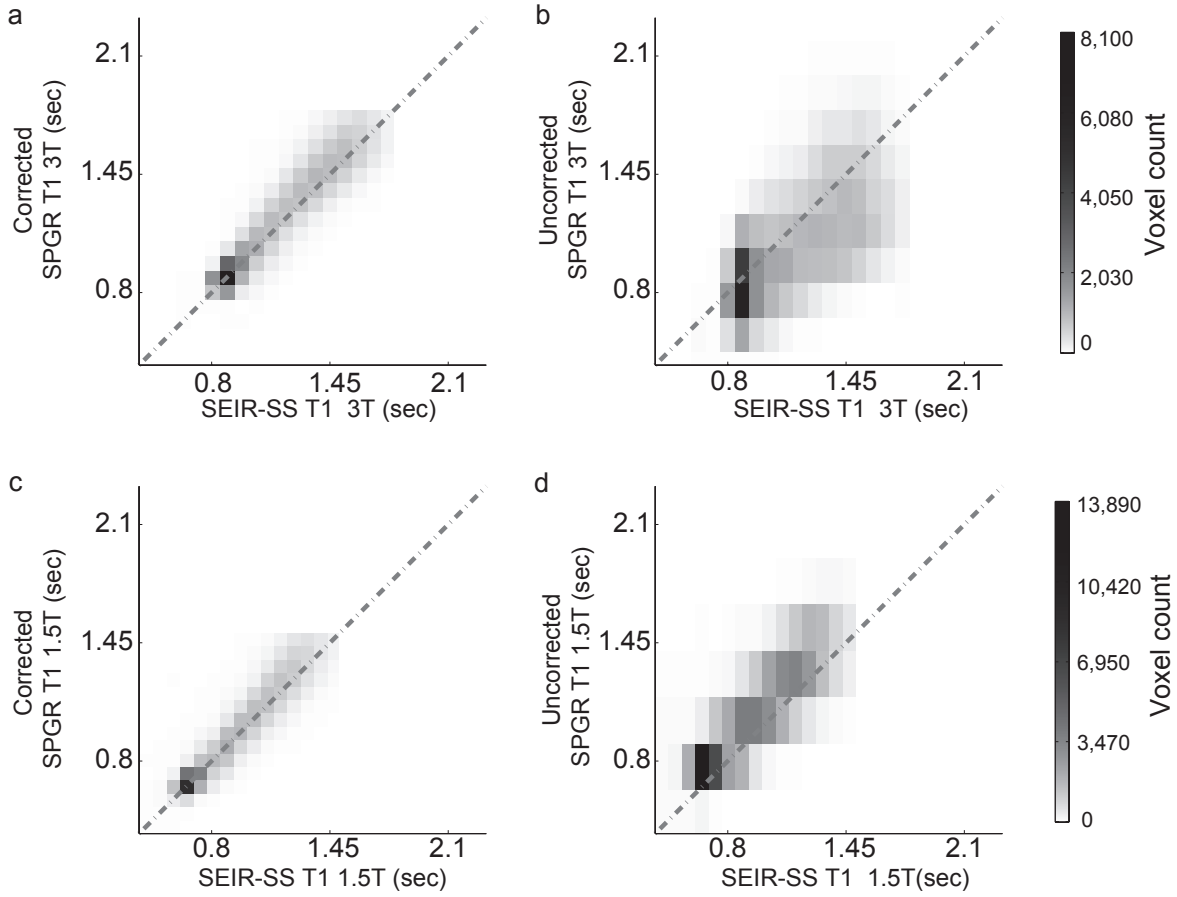

Supplementary Figure 2. T1 mapping using SEIR-SS and spoiled-GE with transmit-coil correction are consistent. (**a**) The scatter plot compares gray and white brain matter T1 values of SEIR-SS with T1 values from transmit-coil corrected spoiled-GE measurements (*n*=3). The data were collected at 3T. The shading indicates the number of measured voxels with that value (scale bar in the right). (**b**) The scatter plot compares the SEIR-SS and uncorrected spoiled-GE estimates in the same three subjects. (**c, d**) The same analyses are shown as in panels A and B, but for two subjects measured at 1.5T. Correcting for transmit-coil imperfections brings the measurements into better agreement. The corrected estimates are near the identity line with mean difference close to zero.

Nature Medicine: doi:10.1038/nm.3390

Reliability of PD and MTV mapping

Accurate MTV estimation depends on both receive- and excite-coil bias corrections. **Figure 1a** shows that a known volume of lipid mixtures can be measured reliably from the M_0 when correcting the coil biases. **Figure 1c,d** shows that after bias corrections the MTV measurements measured with two different coils (32 and 8 channel) agree well. To further evaluate the reliability of the MTV values we estimated the variation in the PD value along a homogeneous agar phantom. The PD value is proportional to MTV (see Methods) therefore we calculate the deviation of the PD values from the mean value. The standard deviation in the homogeneous case is the error matrix of the PD and MTV estimation. **Supplementary Figure 3** shows the distribution of the PD values in the phantom before and after receive-coil correction. The correction reduces the standard deviation of the PD values from 0.27 to 0.005.

One potential concern with our method in human brain is whether T2* effects can be neglected at these short echo times (TE = 2.4 ms). The comparisons in this **Figure 1d** show that this assumption is reasonable: MTV estimates are not influenced by differences in field strength even though brain T2* varies with field strength. The TE in the method is short compared to the water proton T2* (10s of ms) but long compared to semi solid and macromolecule protons T2* (microseconds, [3,4]. Hence, both of these effects are invisible for the 2.4 ms TE.

Nature Medicine: doi:10.1038/nm.3390

Supplementary Figure 3 - Proton density measurement with RF-receive correction

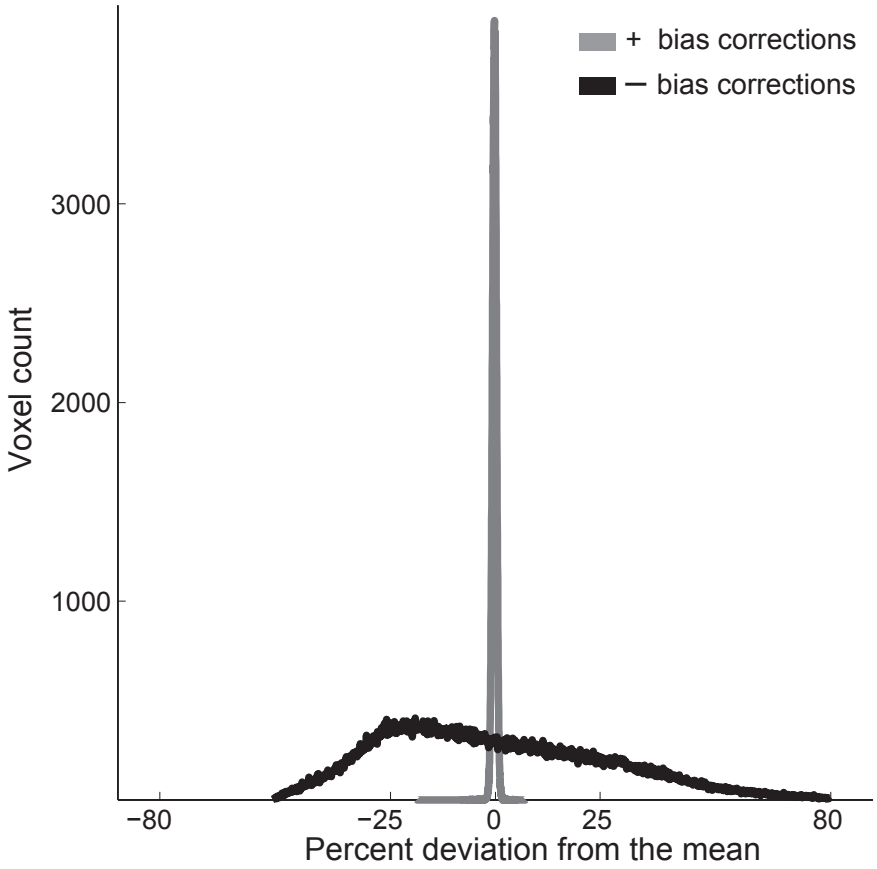

Supplementary Figure 3. Proton density measurement with RF-receive correction is reliable. M_0 values depend on the effects of RF-coil receive gain and proton density. The histogram shows the percent difference between the M_0 values and the mean measured at 3T in a homogeneous agar phantom (black). Without coil correction the values are widely distributed. Correcting for receive-coil gain strongly reduces the M_0 variation (gray). After correction the mean error is close to zero and the standard deviation of the error is reduced from 0.27 to 0.005.

Nature Medicine: doi:10.1038/nm.3390

Reliability of T1 mapping across multiple scans

We measured the reliability of T1 mapping using spoiled-GE across sessions at both 1.5T and 3T (**Supplementary Figure 4**). The agreement as measured by the coefficient of determination is R^2=0.7 in the gray and white matter; the average standard deviation from the mean T1 value is 2.8% in gray and white matter. Those values are close to the measurement noise as defined by bootstrap estimates from multiple repeats in the same scan, where registration is less of an issue (3.5% for whole brain, 2.2% in white matter and up to 28% in CSF).

Next, we tested the effect of the scan parameters, TR, TE and flip angle, on the T1 estimates. The TR affects the signal-to-noise ratio: long T1 and short TR result in a low signal. Therefore, a short TR may bias the estimation toward the low T1 values. **Supplemental Figure 5a** compares the T1 measurements using TR=20 ms with TR=80 ms. The difference between the two estimates is unbiased, and variance is within measurement noise as defined by bootstrap estimates from multiple repeats (not shown).

TE should not affect the T1 estimation as long as the tissue T_2^* is unique. In a voxel that contains tissue types with different T_2^* values, the T1 estimate will be biased towards the value of the tissue with the higher T_2^*. T2 values are not thought to be uniform within the brain [5] and therefore the assumption of a unique T_2^* value can only hold if the T_2^* in the M_0 image is neglected (exp(-T_2^* /TE) ~ 1). **Supplemental Figure 5b** shows that T1 values measured with TE=2.4 ms. or with TE=12 ms. are unbiased and the difference is similar to measurement noise. This validates the assumption that T_2^* effects are negligible.

Variations in flip angle may produce different T1 estimates due to magnetization transfer effects that are not captured in the basic signal equation (Equation 1.1). This effect is substantial only with flip angles larger than those used in this work [6]. **Supplemental Figure 5c** shows that T1 estimates made using different flip angle sets ($\alpha = 3^o, 9^o, 18^o, 26^o$) and ($\alpha = 4^o, 10^o, 20^o, 30^o$) are unbiased and repeats are similar to the measurement noise.

We considered whether the agreement between the spoiled-GE T1 maps and the SEIR-SS (**Supplementary Figure 2**) is due entirely to the excite inhomogeneity bias correction that is based spin-echo inversion recovery (SEIR) with an echo-planar imaging (EPI). To test this idea, we applied a different excite bias correction method that does not rely on SEIR[7]. This method corrects the bias by fitting a low spatial frequency mean field to a brain mask. The bias correction fitted to a white matter mask. Furthermore we calculate

Nature Medicine: doi:10.1038/nm.3390

the mean bias field by adjusting the corrected CSF T1 to be equal to the CSF T1 in the literature (4 sec). As **Supplementary Figure 6** shows the SEIR-SS and spoiled-GE T1 are similar when no SEIR data are used to fit the excite inhomogeneities (R^2=0.60). It is worth noting that this method often works well, but there is a risk that a patient may have a slow variation in real tissue along the brain (like in **Figure 4** and **Supplementary Figure 11**); this might mistakenly be removed by this method.

Supplementary Figure 4 - T1 mapping reliability

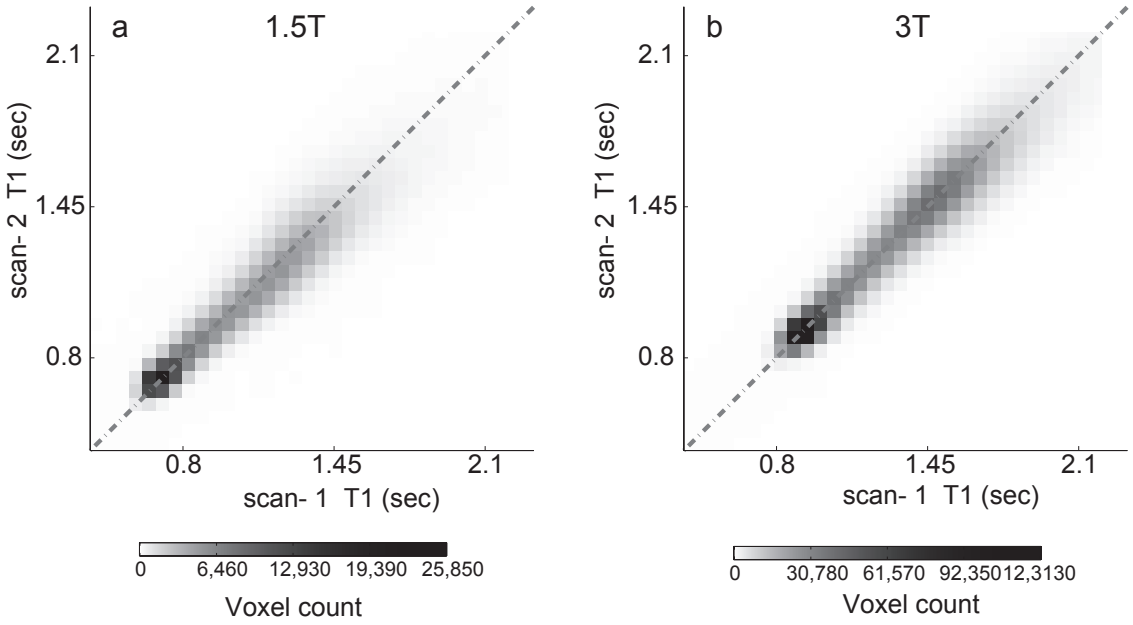

Supplementary Figure 4. T1 mapping using spoiled-GE and transmit-coil inhomogeneity correction is reliable across multiple scan sessions. Scatter plots of the gray and white matter T1 values measured in two scans at 1.5T (**a**) and 3T (**b**) with transmit-coil inhomogeneity correction (*n*=3). Without transmit-coil inhomogeneity correction, the spoiled-GE T1 maps have a systematic bias (not shown). The corrected estimates are near the identity line and the percent error between the two T1 values is unbiased and near zero. Other details as in **Supplementary Figure 2**. See text for details.

Nature Medicine: doi:10.1038/nm.3390

Supplementary Figure 5 - The effect of TR, TE and flip angle on the T1 estimation

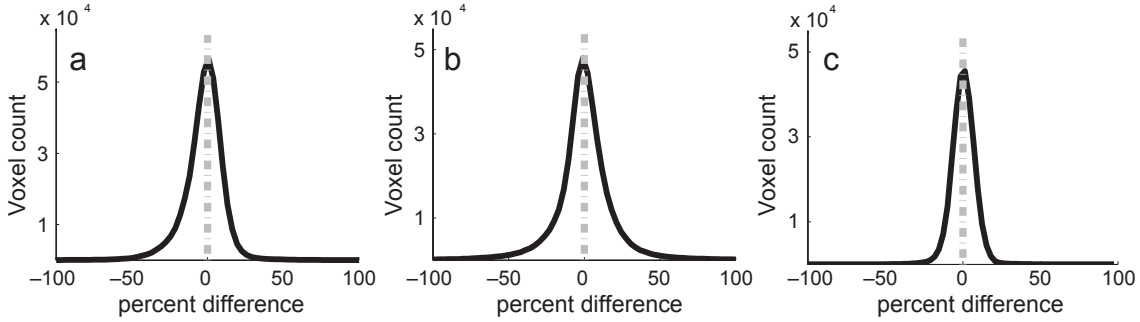

Supplementary Figure 5. The effect of TR, TE and flip angle on the T1 estimation. To test the reliability of the spoiled-GE images T1 mapping, we systematically varied several scan parameters. For each set of parameters, the T1 was estimated and the percent difference between the T1 estimations was calculated. (**a**) The percent difference in the T1 estimation is plotted for one subject scanned with two TR values (20 and 80ms), but otherwise identical parameters. (**b**) The percent difference in the T1 estimation is plotted for one subject that was scanned with two different TE values (2ms and 12ms), but otherwise identical parameters. (**c**) The percent difference in the T1 estimation is plotted for one subject that was scanned with two different flip angles sets ([3^o 9^o 18^o 26^o] and [4^o 10^o 20^o 30^o]), but otherwise identical parameters. See text for details.

Nature Medicine: doi:10.1038/nm.3390

Supplementary Figure 6 - T1 maps using SEIR-SS and spoiled-GE with RF-excite bias by low spatial frequency bias field correction.

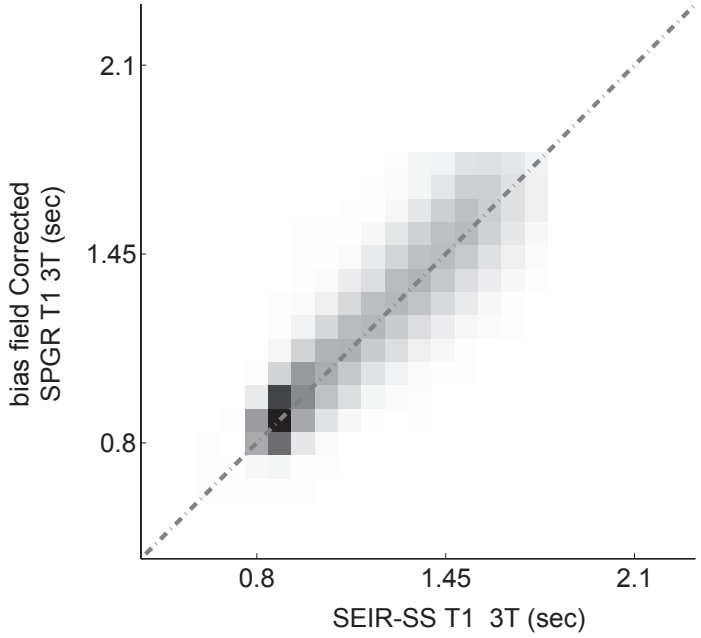

Supplementary Figure 6. T1 maps using SEIR-SS (gold standard) and spoiled-GE with RF-excite bias by low spatial frequency bias field correction are consistent. The scatter plot compares gray and white brain matter T1 values of SEIR-SS with T1 values from transmit-coil corrected spoiled-GE measurements using low spatial frequency bias field. Other details are identical to **Supplementary Figure 2 a**.

Nature Medicine: doi:10.1038/nm.3390

Biophysical modeling of T1 and MTV relations

Variations in T1 values across white matter are largely explained by the variations in tissue volume (**Figure 5**). However, the specific parameters relating T1 and MTV differ between brain structures (**Figure 2**). The T1-TV relationship also depends on the health status of the tissue (**Figure 4** and **Supplementary Figures 11**). What are the biological sources of these variations?

In the following section we use the T1 literature to develop a biophysical model that explains why the parameters of the T1-MTV relationship vary. We build on nuclear magnetic resonance theory to describe a formula that transforms measured T1 values into tissue properties. Hence, the theory converts T1 values, in units of seconds and magnetic field dependent, to a quantitative tissue property. We call the derived tissue property 'the apparent volume of interacting water protons' (VIP). The VIP value has units of volume (ml) and the value is field independent.

By dividing VIP by macromolecular tissue volume (MTV), we estimate the rate of spin-lattice relaxation normalized by tissue volume. We call this ratio the water-surface interaction rate (SIR). We validate these ideas with measurements of VIP and SIR using controlled lipid phantoms with controlled levels of MTV and cholesterol embedded in the lipid membrane. We suggest that SIR may be used to differentiate between brain tissues and assess abnormalities in brain tissues. The biophysical model brings in-vivo clinical imaging a step closer to the biochemistry and biophysics of the underlying brain tissue.

T1 modeling approaches slow vs. fast exchange

Biophysical theory explains T1 relaxation time in brain tissue as arising from multiple mechanisms: the free water protons (free pool) and the protons that interact with the surface of local macromolecules (compartment pools) [8-10]. The water protons in the free pool exchange their energy with the surrounding water relatively infrequently. Changes in the mean field do not have a significant impact on the free water pool T1 value [11].

The protons bordering the macromolecules have a higher probability of exchange with their environment; these protons convert to the lower energy state more rapidly than the free water protons. The mechanisms determining T1 appear to include phenomena such as dipole interaction, proton or molecule exchange, magnetization transfer and possibly slowly diffusing hydration water pools. The T1 value from these compartment pools depends on the mean field [11,12]. For reviews of the theory at this fine scale see Refs[13,14].

The T1 relaxation depends on the properties of the water environments (water compartment pools) in each brain voxel. The interpretation of the T1 relaxation process differs if exchanges between the proton pools are fast or slow with respect to the T1 time constant. In the slow exchange case, T1 is described with multi exponential recovery model. But in the fast exchange case T1 relaxation is expected to follow a mono-exponential recovery [15].

Many investigators report that T1 relaxation in the brain is well described using a mono-exponential model, consistent with the fast exchange model[8-10]. Because measured deviations from the mono-exponential model are small, particularly in white matter, we use the fast exchange formulation to explore the biophysical relation between T1 and MTV. Because there have been some suggestions that the fast exchange model fails under some measurement conditions, we begin by discussing this literature. We then explain how to use the fast exchange model in our theoretical analysis of quantitative tissue properties.

Does et al. [16,17] describe a sequence that measures both T1 and T2 relaxation. In certain biological tissue, they find that the signals can be segregated into three slowly exchanging T2 compartments (i.e. multi-exponential decay). They estimate the T1 value within each T2-defined compartment and report that the T1 values differ. This observation supports a slow-exchange model. But this result was obtained in peripheral nerves of non-human samples both in-vitro [16] and in vivo [17]. The corresponding measurements by this group in brain gray and white matter were well-fit using a single T1 exponential decay consistent with the fast exchange model [17].

Macromolecule and semi-solid water protons might influence T1 relaxation. The T2* of semi-solid protons is on the order of microseconds and can only be detected by sequences using ultra short TE [3,4]. These effects can be neglected in typical imaging sequences using millisecond range for the TE parameter.

Semi-solid bound protons might influence the T1 relaxation of the observed water protons via indirect mechanisms. The quantitative MT literature develops a theory that relates the observed T1 value (T1obs) to the T1 values of two different pools, T1a (water pool) and T1b (bound pool), based on a slow-exchange model [18,19,20] According to the theory T1obs is not a simple mixture of T1a and T1b but depends on the size of the pools and the between-pool mixing rates. Under this assumption T1a is a mixture of water pools that have a fast exchange, but the measured T1obs is also influenced by slow exchanges with the bound pool.

Several quantitative MT studies report measurements of 1/T1obs and estimates of 1/T1a based on a quantitative MT model. **Supplementary Figure 7** plots values taken from tabulated data [18,21-23]. The data and estimates in the figure were obtained using MR techniques made with short TR (e.g., spoiled-GE) and long TR values. The data were also obtained using a variety of substrates (Agar, in vitro tissue, and in vivo brain tissue).

The equality between T1obs and T1a shows that for the conditions in these papers there is no detectable influence of T1m on the observed T1. These results agree with **Supplementary Figures 2**,**6** that the measured T1 with SEIR method and with spoiled-GE are identical.

Ou et al. [6] perform a useful simulation with the goal of understanding the implications of their model would be for conventional spoiled-GE measurements, such as we use in the proposed method. Deoni et al. [24] also simulated slow exchanging water pools that resemble the measured T2 slow exchanging myelin and non-myelin water pools that were previously described [5]. Both simulations suggest that there is a range of TR and flip angles that inappropriately fit a mono-exponential T1 decay to slow exchanging multi compartment systems, and that in these conditions the result will be a biased T1 estimate. We performed measurements varying TR and flip angle to look for support for the predictions from the slow exchange model. **Supplementary Figure 5a** shows that the estimated T1 estimates are invariant over a large range of relevant TR values (TR=10ms vs. TR= 80ms). Similarly, **Supplementary Figures 2,6** shows that the T1 spoiled-GE (TR of 10ms in 1.5T and 14ms in 3T) resembles the SEIR single exponent T1 with TR of 3sec. Finally, **Supplementary Figure 5c** shows that variation in across the flip angle range used in our measurements produced an invariant T1 estimate as well.

Mulkern et al. [25] explored slow exchanging T1 compartments in the human brain. They defined different cellular compartments using diffusion measurements obtained over a range of b-values. The diffusion data could be partitioned into different compartments. However, they found only a single T1 for the different diffusion-defined compartments. They provide a model showing how it is possible that T2 and diffusion data appear to be segregated into multiple compartments (slow exchange), while T1 exchange remains consistent with a fast-exchange, single exponential decay.

In complex systems, all models are phenomenological, and there is a trade-off between simplicity and detail. We think the literature and our data show that the observed T1 in brain tissue is well approximated by a mono-exponential decay[8,9], as predicted by the fast exchange model. We use this model to interpret the data. This approach values speed of the acquisition, robustness of the calculation, and simplicity of the interpretation.

Supplementary Figure 7 - Literature review comparing T1 observed with T1 of water

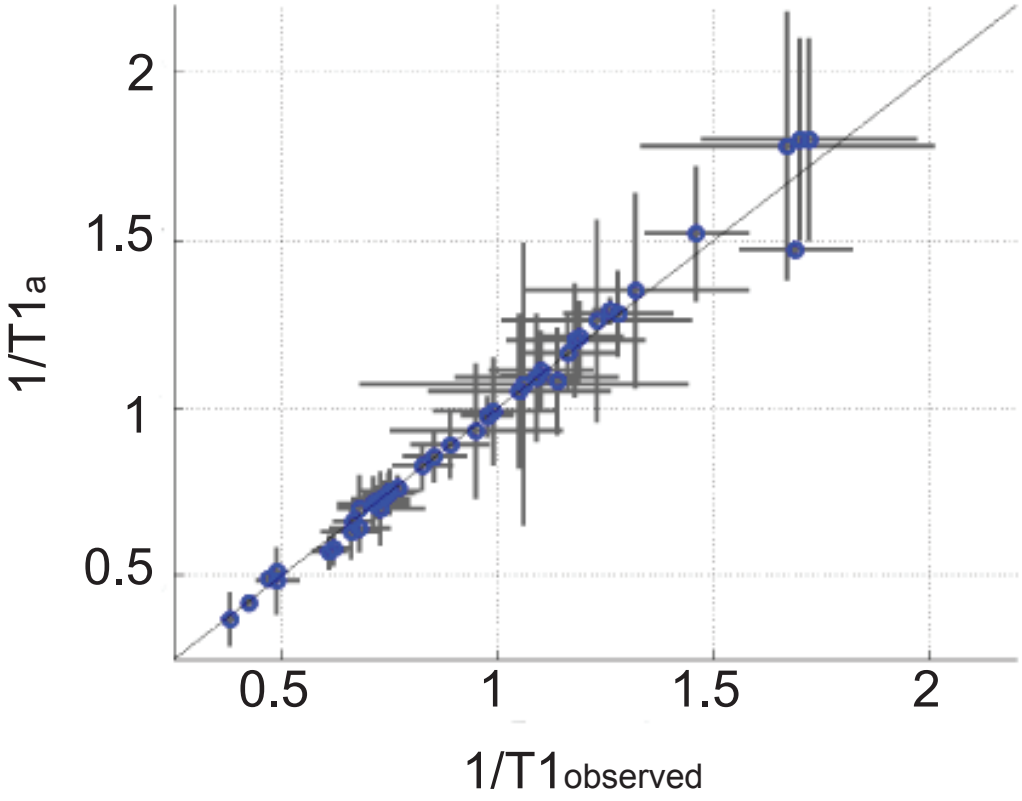

Supplementary Figure 7. Literature review comparing T1 observed with T1 of water. Several quantitative MT studies report measurements of $1/T1_{observed}$ and the relaxation estimates of the water pool mixture $1/T1_a$ based on a quantitative MT model. The figure plots values taken from printed tables [18,21-23]. The data and estimates were obtained using MR measurements with short TR (e.g., spoiled-GE) and long TR values. The data were obtained using a variety of substrates (Agar, in vitro brain, in vitro fresh beef, and in vivo brain tissue). Error bars from different sources represent different ranges (gray). The estimates $1/T1_{observed}$ and $1/T1_a$ are near the identity line (black). The outlier is the in-vitro fresh beef.

Nature Medicine: doi:10.1038/nm.3390

The single exponential decay for complex biology system can be explained by the Zimmerman et al. [15] formalism. They showed that when there is a fast exchange of protons between compartments, the relaxation of the entire sample is a single exponential. The time constant of the entire sample is equal to the weighted sum (C_i) of each individual compartment's time constant ($\frac{1}{T1_{c,i}}$) and the free pool, ($\frac{1}{T1_f}$)

$$\frac{1}{T1} = \sum_{i=1}^{n} C_i \frac{1}{T1_{c,i}} + (1 - \sum_{i=1}^{n} C_i) \frac{1}{T1_f} \qquad 2.1$$

Deriving VIP from T1 and MTV

Below we suggest a biophysical model that characterizes the brain tissue relaxation with the fast exchange assumption. A summary of the model is in **Supplementary Figure 1**.

The protons bordering the macromolecules interact with different proteins, lipid surfaces and paramagnetic ions, each of which has a unique T1 value ($T1_{c,i}$). These values tend to be significantly shorter than $T1_f$ and thus the T1 of each voxel is significantly influenced by the T1 in these compartments. We aim to characterize the volume of these interacting water protons (VIP).

If we define $T1_C$ as

$$\frac{1}{T1_C} = \sum_i C_i \frac{1}{T1_{c,i}} \Big/ \left(\sum_i C_i \right) \qquad 2.2$$

We can rearrange the terms

$$\left(\sum_i C_i \right) \frac{1}{T1_C} = \sum_i C_i \frac{1}{T1_{c,i}} \qquad 2.3$$

We call the sum of the concentrations 'fraction of interacting water protons '(FIWP)

$$\sum_i C_i = FIWP$$

Substituting this term we re-write Equation 2.1 as:

$$\frac{1}{T1} = FIWP \frac{1}{T1_C} + (1 - FIWP) \frac{1}{T1_f} \qquad 2.4$$

We can rearrange Equation 2.4

$$\text{FIWP} = \frac{\frac{1}{T1} - \frac{1}{T1_f}}{\frac{1}{T1_C} - \frac{1}{T1_f}} \qquad 2.5$$

To estimate the apparent volume of interacting water protons VIP in a voxel, we multiply *FIWP* by the fraction of water in the voxel $WVF = 1 - MTVF$ and the voxel volume, V

$$VIP = FIWP(1 - MTVF)V \qquad 2.6$$

Hence, we can estimate VIP from the measurements of T1 and PD and the values $T1_f$ and $T1_C$ (Equations 2.5, 2.6). The free pool $T1_f$ can be theoretically estimated [11] and has been measured to be $T1_f$ ~ 4.3sec in the brain CSF at body temperature [26]. The open question is how to estimate $T1_C$.

Deriving the compartment characteristic $T1_C$ from in-vivo data

The $T1_C$ value summarizes the T1 values in all the tissue compartments; the value is what we expect to find if we extract brain tissue, pump out the free water, and measure T1 as a function of field strength at body temperature. Fullerton et al. [27] provide an insight into the value of $T1_C$. They measured a wide range of biological tissue in vitro after pumping out the free water. They found that the $T1_C$ values depend linearly on the Larmor frequency (L, MHz)

$$T1_C = a_1 L + a_2 \qquad 2.7$$

We can estimate the parameters in this relationship in vivo using the following method: At two Larmor frequencies (magnetic field strengths), we measure T1(L) in a subject with N brain voxels. This yields 2N measurements. There is one unknown *FIWP* value for each voxel (Equation 2.4), and two unknown values (a_i) for the entire data set (Equation 2.7). With N+2 unknowns and 2N measurements, we can estimate the parameters (a_i) within the range of measured field strengths.

We modeled the T1 value as depending on two terms. The first term is the contribution from the protons adjacent to macromolecules, $T1_c$, which varies linearly with field strength over a modest range (0.5-3T). The second term is the contribution from the free water, $T1_f$ which is field strength independent.

To estimate the parameters we used T1 maps of two subjects in 1.5T and 3T. The 3T maps were co-registered to the 1.5T maps and all data were interpolated to 2 mm isotropic resolution.

We estimated the coefficients by choosing 100 voxels randomly from the white matter of those two subjects and fitting the 200 T1 measurements with the two parameters in Equation 2.7 and 100 *FIWP* parameters (Equation 2.4). We repeated the fitting with 1500 samples and calculated the mean and standard deviation of the two linear model coefficients in Equation 2.8. The estimated coefficients are a1 = 0.934±0.031 and a2 = 93.3±2.1.

$$T1_C = (0.934L + 93.3)\times 10^{-3} \qquad 2.8$$

The $T1_C$ parameter has units of seconds and the Larmor frequency (L) is specified in MHz.

To validate the theoretical modeling and the measurement procedures, we tested the prediction of T1 measurements across field strengths using the model. The model used data from 1.5T and 3T to estimate the linear coefficients. We then used the 1.5T data to predict independent data sets obtained at 0.5T (**Supplementary Figure 9b**). We then collected an independent data set at 1.5T and 3T on a third subject. Using the parameters from the first two subjects, we used the 1.5T data to predict the 3T data (**Supplementary Figure 9c**). Similar co-registration and interpolation as describe above were used also for the testing data sets. The predicted T1 values agree well with the measured T1 values with a high coefficient of determination ^{2} and small RMSE (see **Supplementary Figure 9** legend). Hence, the theory enables us to remove the instrument-dependence of the T1 measurements and derive the instrument independent anatomical measures.

We can assemble the equations into a single unified expression that estimates the VIP assuming that T1 in the tissue compartment equals $T1_C$

$$VIP = \frac{\left(\frac{1}{T1(L)} - \frac{1}{T1_f}\right)}{\left(\frac{1}{T1_C(L)} - \frac{1}{T1_f}\right)} \times (1 - MTVF) \times V \qquad 2.9a$$

Including the specific parameters, we have a final expression for VIP.

2.9b $$VIP = \frac{\left(\frac{1}{T1(L)} - \frac{1}{4.3}\right)}{\left(\frac{10^3}{0.934L + 93.3} - \frac{1}{4.3}\right)} \times (1 - MTVF) \times V$$

Brain tissue characterization using MTV and VIP

The VIP value has several properties that make it a useful complement to T1 or T1-weighted measurements for brain research and clinical assessment. The VIP units are volume and thus they are independent of field strength (over the range of 0.5T-3T); in contrast, T1 or T1-weighted values depend on field strength.

An intuition concerning the physical meaning of VIP is this: After absorbing RF energy, the excited water protons give up their energy to the environment (lattice). The VIP measures the volume of excited water protons that relax by interacting with the lattice. Thus, the VIP depends on the tissue volume as well as the efficiency with which the water protons and tissue interact to shorten the relaxation time.

In the first experiments we measured MTV phantoms with controlled volumes and surface properties. Specifically, we constructed phosphatidylcholine lipid mixtures with and without cholesterol embedded in the lipid membrane (**Figure 1a**). In **Supplementary Figure 8** we calculate the VIP for the two lipid mixtures. Like the MTV values, the VIP values increased with lipid volume for both mixtures. Unlike MTV, the VIP depends on the cholesterol content of the lipid membrane. The cholesterol content changes the slope of the dependence between VIP and lipid volume. This agrees with earlier work showing that different macromolecules [28] and in particular cholesterol [29] change the ability of the surface to reduce T1 and therefore VIP estimation. It is also in agreement with the idea that the apparent VIP summarizes macromolecule and water interface volume as well as the reactivity of these surfaces.

An interesting statistic, that characterizes the nature of the lipid membrane, is to normalize the VIP by the tissue volume. This statistic summarizes the proton-surface interaction rate correcting for total tissue volume. The ratio of VIP and MTV for membranes with cholesterol is 0.16; without cholesterol the ratio is 0.02.

We refer to the ratio of VIP and MTV as the surface and water interaction rate (SIR).

2.11 $$SIR = VIP/MTV$$

High SIR means high efficiency of the water-surface interaction that speeds the T1 relaxation. SIR measures differences in the tissue composition, as we illustrated

empirically by showing the effect of embedded cholesterol on the T1 of lipid membranes (**Supplementary Figure 8**)

DI values (described in the Results Section) quantify the deviation between the measured T1 values from the value predicted from the amount of tissue. In a similar way, the biophysical modeling approach of MTV and SIR enables to identify the brain regions that differ by their T1 relaxation after accounting for the MTV effects. Like DI, SIR values differ between gray, white and thalamic regions (0.479, 0.493, 0.543 and an average standard error of 0.007). The values also differ between normal white matter and MS patients' white matter (~5% and higher SIR in some individuals with multiple sclerosis white matter).

Advantage and limitations in T1 biophysical modeling

The biophysical modeling presented in this appendix offers a complementary way to think about the measurements compared to the data driven approach in the main text. The modeling relates the measurements to specific tissue properties, i.e. the efficiency of the water-surface interaction in accelerating the water T1 relaxation. Furthermore, the biophysical model allows for a field independent analysis (between 0.5-3T). The data driven approach has the advantage of being free from assumptions and therefore it is less likely to lead to a misrepresentation of the underlying processes.

There are a small number of key assumptions to the model. First, the fast exchange assumption[15] (Equation 2.1) may not correctly model the interactions between distinct tissue pools[16,30]; in the case of slow exchange the expected longitudinal relaxation differs from a single exponential (see discussion above). Second, we assumed a linear dependence of the apparent combined relaxation time of all the compartments ($T1_C$) with the magnetic field (Equation 2.7). The nuclear magnetic resonance theory and measurements suggest that this relationship is nonlinear over a large range, but it is close to linear in the restricted range from 0.5T to 3T [10,11,27 31].

Even if these limitations exist at the nanometer scale, it is still plausible that the first-order model of VIP and SIR based on the fast exchange model is a useful approximation for human neuroimaging data acquired at the millimeter scale. For the measurements we have obtained, the model is quite accurate. Further work will be needed to establish the limitations of the model and where it might fail.

Nature Medicine: doi:10.1038/nm.3390

Supplementary Figure 8- VIP for lipid mixture phantoms

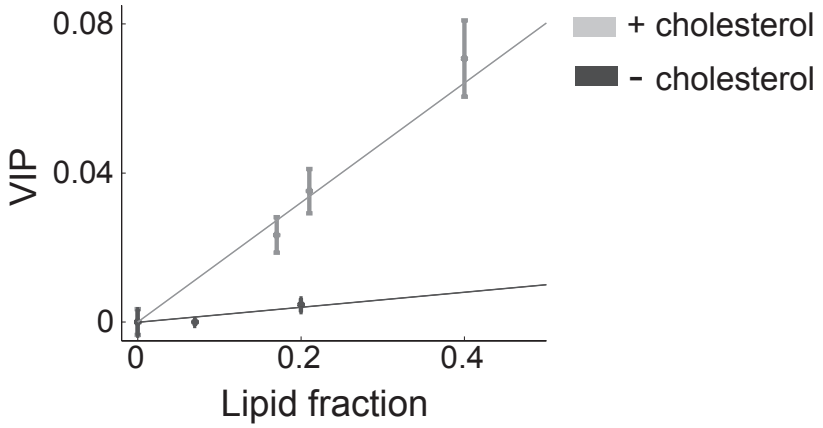

Supplementary Figure 8. VIP for lipid mixture phantoms. The apparent volume of interacting water protons (VIP) measured using a lipid mixture with (gray) and without (black) cholesterol. The vertical bars are the standard deviation of the measurement. The average standard deviation is smaller than 0.005. The VIP of both lipid mixtures increases with lipid volume, but the lipids with cholesterol (30% weight) increase at a much higher rate. The VIP is a water proton volume that interacts with the macromolecules. Therefore the VIP values are dependent on both the volume of interactions with the water (the macromolecules volume) and interaction efficiency (the kind of macromolecules). The ratio of the VIP to the lipid volume (the slope) divides out the macromolecule volume aspects; hence, this ratio measures surface and water interaction rate (SIR). The MTV values of the same samples are shown in **Figure 1a**.

Nature Medicine: doi:10.1038/nm.3390

Supplementary Figure 9- T1 dependence on field strength predictions

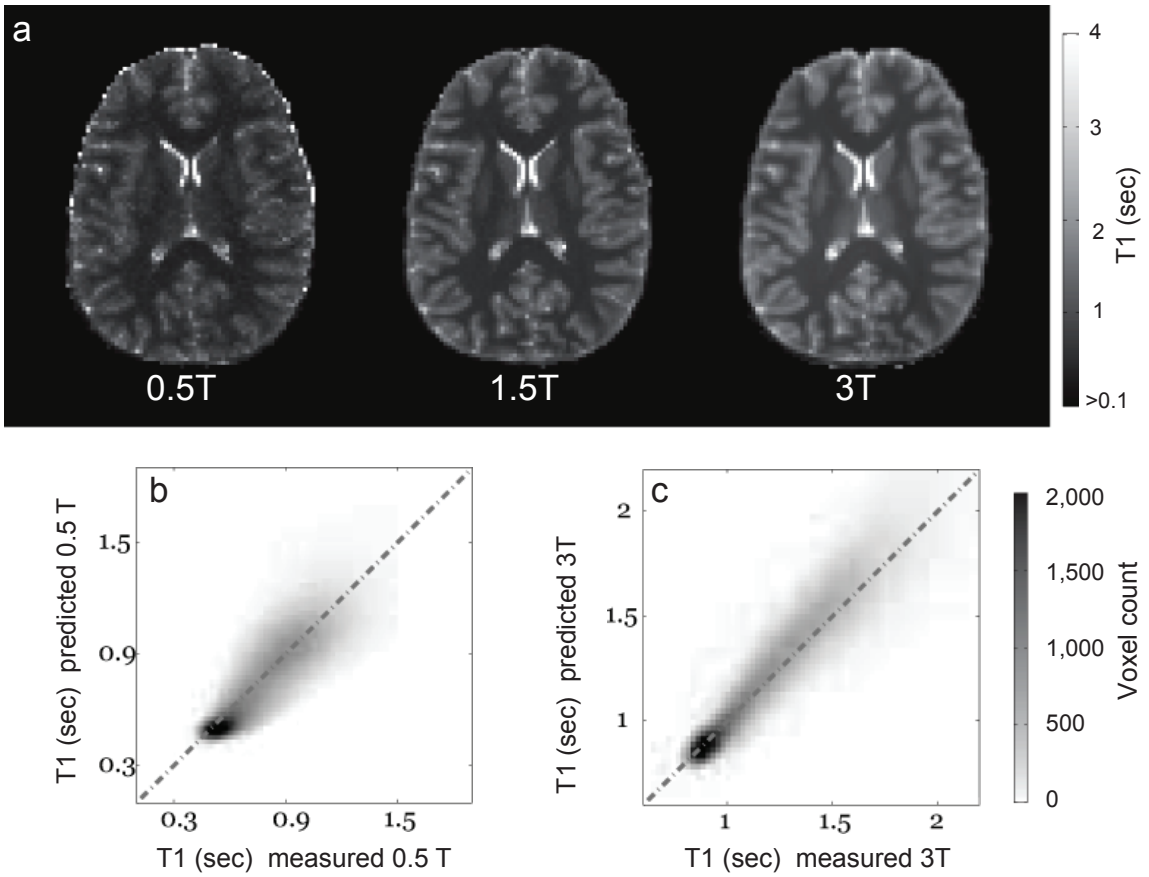

Supplementary Figure 9. T1 dependence on field strength predictions**.** (**a**) An axial brain slice showing T1 maps in the same subject measured at 0.5T, 1.5T and 3T. The three images were co-registered and resampled to a resolution of $2mm^3$. The T1 values increase with field strength. The biophysical T1 theory predicts how T1 values changes with field strength. (**b**) The scatterplot compares T1 values measured at 0.5T and the predicted T1 values based on measurements made at 1.5T within the gray and white matter of a single subject. Note that these 0.5T data was not used to fit the T1 model. R^2 = 0.461; the RMSE is 0.064 sec in white matter and 0.15 sec in gray matter. (**c**) Scatterplot of T1 values measured at 3T and the predicted T1 values from measurements made at 1.5T within the gray and white matter of a single subject. Note that the 1.5T or 3T data were not used to fit the T1 model. R^2 = 0.735; the RMSE is 0.09 sec in white matter and 0.15 sec in gray matter.

Nature Medicine: doi:10.1038/nm.3390

MTV Relationship to other quantitative MRI methods

MR pulse sequences can be adjusted to measure a variety of biophysical tissue properties. There is an interesting collection of MRI methods under development to probe tissue properties, and the MTV measure is a member of this collection. In this section we discuss the similarities and differences between these approaches. These different MR measurements can be viewed as complementary to one another. Taken together, they inform us about tissue integrity and ultimately about the relationship between brain structure and function.

Diffusion

Diffusion imaging is the most widely used biophysical measure of brain structure [32,33]. Diffusion imaging measures the statistics of water displacement, and these statistics inform us about the orientation of the nearby membrane boundaries. This information can be useful to diagnose problematic tissue at a local scale. By aggregating diffusion information across multiple voxels, it is possible to estimate the locations of major white matter tracts [34-36].

Membrane orientation, density and permeability all influence the diffusion signal. The heterogeneity of biological factors that drive the diffusion signal limits the interpretation of diffusion measurements [37,38]. **Figure 4** shows that there is an opportunity to integrate MTV values with diffusion signals to separate these different contributions.

Statistically, the MTV difference between subjects is greater than the difference within each subject's tract. The FA variations within subjects are greater than those between subjects. Therefore MTV values may be a particularly useful measure to understand individual differences. Indeed ranking of subjects by the measurement in the first half of the tract CST (**Figure 4b,c**) accurately predicts the ranking in the second half for MTV ($r=0.93$, $p<0.001$, but the rank ordering prediction is less predictive for FA ($r=0.51$, $p<0.05$).

Quantitative Magnetization Transfer

The bound pool fraction (BPF) [18,23,39] method uses a quantitative magnetization transfer (MT) pulse sequence and a computational model to estimate the non-water protons bound to macromolecules. This method measures the difference in the magnetic relaxation when off-resonance MT pulses at different strengths are added to a constant on-resonance pulse. Alternatively BPF can be measured with on-resonance multi-exponential decay with a modified fast inversion recovery sequence [20].

The MT signal can be interpreted quantitatively as measuring the number of protons bound to macromolecules. It is not yet certain whether the signal depends on the volume of the membranes or on their surface area [40].

We made BPF measurements on 4 of the subjects in this study. Specifically, we implemented the pulse sequences and post-processing needed to measure BPF based on Yarnykh's method [41]. The BPF values are moderately correlated with MTV values r=0.52 across all brain voxels and r=0.3 in white matter. The voxel by voxel correlation between MTVF and BPF is low. One likely explanation is that the BPF method itself has low scan-to-scan reliability[42]. To improve the reliability, we measured a summary statistic of the mean BPF value along a fiber track (**Supplementary Figure 10**). In this case the correlation coefficients increase for MTVF (0.9; $p < 0.001$). These higher correlations suggest that the BPF measurements are closely related to MTV the value.

For farther discussion about quantitative magnetization transfer relation to T1 see the above section 'T1 modeling approaches slow vs. fast exchange 'and **Supplementary Figure 7**.

T2 -Myelin Water Fraction

The myelin water fraction (MWF) is derived through fitting T2 relaxation using a model comprising multiple exponential components. The analysis typically estimates three T2 time constants that are attributed to different tissue environments. The fast decay signal is thought to represent the myelin water fraction [5]. This method requires many acquisitions and thus a relatively long time to estimate the T2 relaxation function for a full brain scan.

We can compare MWF values with MTV values based on published data. Specifically, we found three articles that tabulate MWF values along with PD values [43-45]. These tables describe the mean values in 20 ROIs from the brains of controls and MS patients. We can compute the VIP values from the tabulated PD and data for each of these ROIs. The correlation (r) of MWF and MTV is 0.79 and is highly significant ($p < 0.002$). These correlations suggest that the MWF measurement is related to MTV values.

Supplementary Figure 10 – The correlation between the mean MTVF and the bound pool fraction (BPF) in white matter tracts

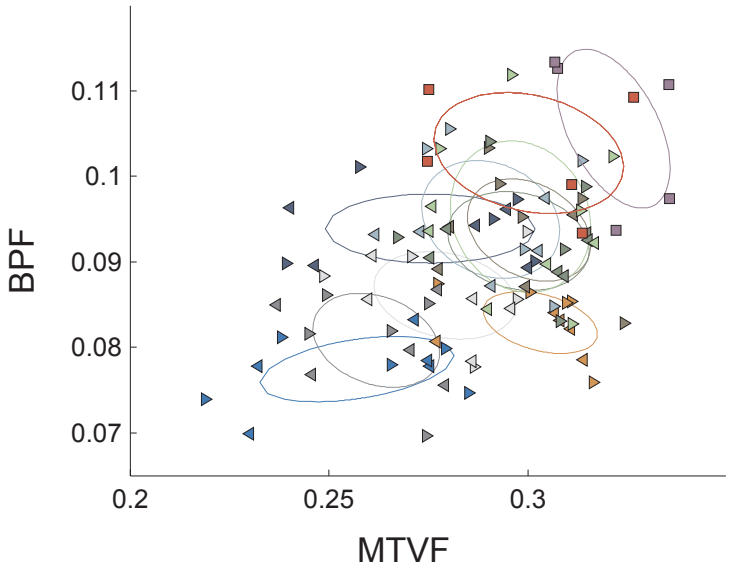

Supplementary Figure 10. The mean MTVF and the bound pool fraction (BPF) in white matter tracts. MVTF and the BPF measurements averaged across major white matter fascicles. The two major fascicles that form the splenium and genu of the corpus callosum (forceps major in red and minor magenta, respectively) are shown with squares. For the nine symmetric tracts, each is shown in a different color and left and right hemispheres are indicated with a left- or right-pointing triangle. There were no obvious asymmetries, so we fit covariance ellipses to the combined data across hemisphere. The correlation coefficients between the fascicles MTVF and BPF for those five subjects is 0.9; $p < 0.001$. The fascicles list: Arcuate in light great, Superior longitudinal in dark green, Uncinate in dark gray, Thalamic radiation in light gray, Cingulum (Hippocampus) light blue, Cingulate in dark blue, Inferior fronto-occipital in cyan and Cortico-spinal in brown. Both the BPF and WVF map calculate from data that was published elsewhere[42]. This database acquisitions parameters are different than the one suggested in this manuscript, therefore to calculate MTVF for this dataset the RF-excite correction was done according to [7] and the RF-receive correction according to [46].

Nature Medicine: doi:10.1038/nm.3390

Supplementary Figure 11– Tissue abnormalities in individuals with multiple sclerosis

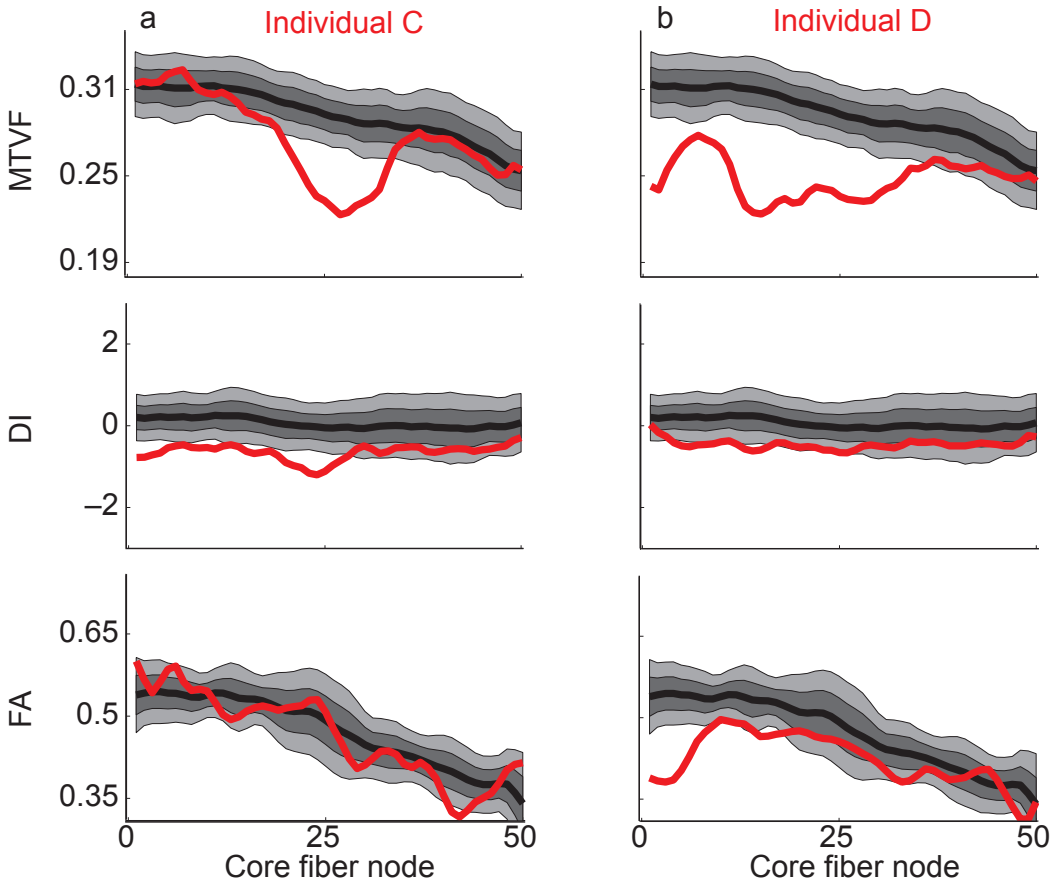

Supplementary Figure 11. Tissue abnormalities in individuals with multiple sclerosis.(**a**) The MTV, DI and FA values along the right ILF (inferior longitudinal fasciculus) in individual-C (red) compared with the distribution of measurements from controls (*n*=16). The black curve represents the mean along the 50 core fiber nodes. The lighter shades show the [25, 75] and [10, 90] percentiles. Both subjects have a large reduction in MTVF at some locations along the ILF. Individual-C also has diffuse reduction in DI values; (**b**) Individual-D has only a minor reduction in DI that suggests differences in their disease stage. Individual-D also some deviations from the control FA values, while individual-C is in the normal range throughout the ILF.

Nature Medicine: doi:10.1038/nm.3390

Supplementary Figure 12 – T1-weighted and FLAIR axial images in two individuals with multiple sclerosis

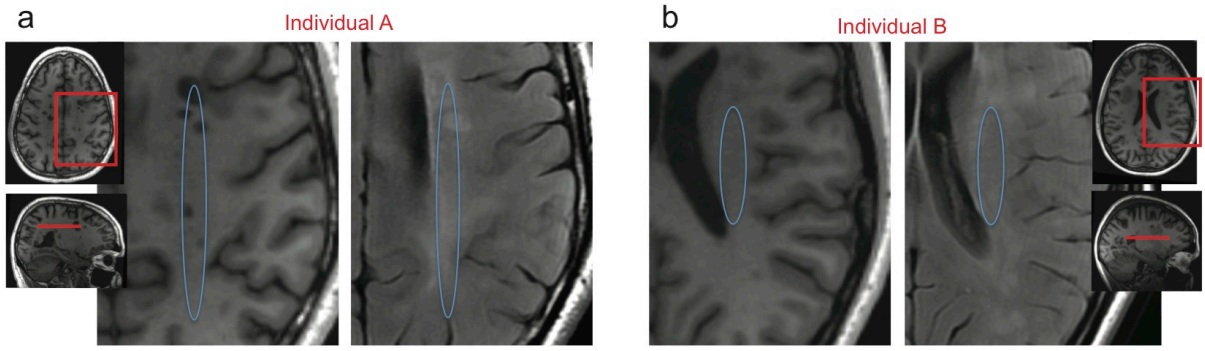

Supplementary Figure 12. T1-weighted and FLAIR axial images in in two individuals with multiple sclerosis. (**a**) The location of the axial images is shown in the inset images. The plane cuts through the CST (blue oval). The plane is the same as shown with an arrow for individual-A at **Figure 4d**. (**b**) The same but for the second individual-B in **Figure 4e**. In this individual the CST region appears normal in the T1-weighted and FLAIR images.

Nature Medicine: doi:10.1038/nm.3390

References

1. Barral, J.K.*, et al.* A robust methodology for in vivo T1 mapping. *Magn Reson Med* **64**, 1057-1067 (2010).
2. Steel, R.G.D. & Torrie, J.H. *Principles and procedures of statistics : a biometrical approach*, (McGraw-Hill, New York, 1960).
3. Horch, R.A., Gore, J.C. & Does, M.D. Origins of the ultrashort-T2 1H NMR signals in myelinated nerve: a direct measure of myelin content? *Magn Reson Med* **66**, 24-31 (2011).
4. Tyler, D.J., Robson, M.D., Henkelman, R.M., Young, I.R. & Bydder, G.M. Magnetic resonance imaging with ultrashort TE (UTE) PULSE sequences: technical considerations. *J Magn Reson Imaging* **25**, 279-289 (2007).
5. MacKay, A.*, et al.* In vivo visualization of myelin water in brain by magnetic resonance. *Magn Reson Med* **31**, 673-677 (1994).
6. Ou, X. & Gochberg, D.F. MT effects and T1 quantification in single-slice spoiled gradient echo imaging. *Magn Reson Med* **59**, 835-845 (2008).
7. Weiskopf, N.*, et al.* Unified segmentation based correction of R1 brain maps for RF transmit field inhomogeneities (UNICORT). *Neuroimage* **54**, 2116-2124 (2011).
8. Bottomley, P.A., Foster, T.H., Argersinger, R.E. & Pfeifer, L.M. A review of normal tissue hydrogen NMR relaxation times and relaxation mechanisms from 1-100 MHz: dependence on tissue type, NMR frequency, temperature, species, excision, and age. *Med Phys* **11**, 425-448 (1984).
9. Rooney, W.D.*, et al.* Magnetic field and tissue dependencies of human brain longitudinal 1H2O relaxation in vivo. *Magn Reson Med* **57**, 308-318 (2007).
10. Mansfield, P. & Morris, P., G. NMR imaging in biomedicine. (Academic Press, London, England, 1982).
11. Boloembergrn, N., Purcell, E.M. & Pound, E.V. Relaxtion effects in nuclear magnetic resonance absorption. *Physical Review* **73**, 679-714 (1948).
12. Nelson, T.R. & Tung, S.M. Temperature dependence of proton relaxation times in vitro. *Magn Reson Imaging* **5**, 189-199 (1987).
13. Caluccia, L. & C., F. Proton longitudinal relaxation coupling in dynamically heterogeneous soft systems. *Progress in Nuclear Magnetic Resonance Spectroscopy* **55**, 296-323 (2009).
14. Halle, B. Molecular theory of field-dependent proton spin-lattice relaxation in tissue. *Magn Reson Med* **56**, 60-72 (2006).
15. Zimmerman, J.R. & Brittin, W.E. Nuclear Magnetic Resonance Studies in Multiple Phase Systems: Lifetime of a Water Molecule in an Adsorbing Phase on Silica Gel. *J. Phys. Chem.* **61**, 1328–1333 (1957).
16. Does, M.D., Beaulieu, C., Allen, P.S. & Snyder, R.E. Multi-component T1 relaxation and magnetisation transfer in peripheral nerve. *Magn Reson Imaging* **16**, 1033-1041 (1998).

17. Does, M.D. & Gore, J.C. Compartmental study of T(1) and T(2) in rat brain and trigeminal nerve in vivo. *Magn Reson Med* **47**, 274-283 (2002).
18. Henkelman, R.M*., et al.* Quantitative interpretation of magnetization transfer. *Magn Reson Med* **29**, 759-766 (1993).
19. Sled, J.G. & Pike, G.B. Quantitative interpretation of magnetization transfer in spoiled gradient echo MRI sequences. *J Magn Reson* **145**, 24-36 (2000).
20. Gochberg, D.F. & Gore, J.C. Quantitative imaging of magnetization transfer using an inversion recovery sequence. *Magn Reson Med* **49**, 501-505 (2003).
21. Cercignani, M*., et al.* Three-dimensional quantitative magnetisation transfer imaging of the human brain. *Neuroimage* **27**, 436-441 (2005).
22. Ramani, A., Dalton, C., Miller, D.H., Tofts, P.S. & Barker, G.J. Precise estimate of fundamental in-vivo MT parameters in human brain in clinically feasible times. *Magn Reson Imaging* **20**, 721-731 (2002).
23. Sled, J.G. & Pike, G.B. Quantitative imaging of magnetization transfer exchange and relaxation properties in vivo using MRI. *Magn Reson Med* **46**, 923-931 (2001).
24. Deoni, S.C., Rutt, B.K. & Jones, D.K. Investigating the effect of exchange and multicomponent T(1) relaxation on the short repetition time spoiled steady-state signal and the DESPOT1 T(1) quantification method. *J Magn Reson Imaging* **25**, 570-578 (2007).
25. Mulkern, R.V*., et al.* Multi-component apparent diffusion coefficients in human brain: relationship to spin-lattice relaxation. *Magn Reson Med* **44**, 292-300 (2000).
26. Hopkins, A.L., Yeung, H.N. & Bratton, C.B. Multiple field strength in vivo T1 and T2 for cerebrospinal fluid protons. *Magn Reson Med* **3**, 303-311 (1986).
27. Fullerton, G.D., Cameron, I.L. & Ord, V.A. Frequency dependence of magnetic resonance spin-lattice relaxation of protons in biological materials. *Radiology* **151**, 135-138 (1984).
28. Kucharczyk, W., Macdonald, P.M., Stanisz, G.J. & Henkelman, R.M. Relaxivity and magnetization transfer of white matter lipids at MR imaging: importance of cerebrosides and pH. *Radiology* **192**, 521-529 (1994).
29. Koenig, S. Cholesterol of myelin is the determinant of gray-white contrast in MRI of brain. *Magn Reson Med* **20**, 285-291 (1991).
30. Prantner, A.M., Bretthorst, G.L., Neil, J.J., Garbow, J.R. & Ackerman, J.J. Magnetization transfer induced biexponential longitudinal relaxation. *Magn Reson Med* **60**, 555-563 (2008).
31. Diakova, G., Korb, J.P. & Bryant, R.G. The magnetic field dependence of water T1 in tissues. *Magnetic Resonance in Medicine* **68**, 272-277 (2012).
32. Moseley, M.E*., et al.* Early detection of regional cerebral ischemia in cats: comparison of diffusion- and T2-weighted MRI and spectroscopy. *Magn Reson Med* **14**, 330-346 (1990).
33. Basser, P.J., Mattiello, J. & LeBihan, D. MR diffusion tensor spectroscopy and imaging. *Biophys J* **66**, 259-267 (1994).

34. Mori, S., Crain, B.J., Chacko, V.P. & van Zijl, P.C. Three-dimensional tracking of axonal projections in the brain by magnetic resonance imaging. *Ann Neurol* **45**, 265-269 (1999).
35. Conturo, T.E.*, et al.* Tracking neuronal fiber pathways in the living human brain. *Proc Natl Acad Sci U S A* **96**, 10422-10427 (1999).
36. Basser, P.J., Pajevic, S., Pierpaoli, C., Duda, J. & Aldroubi, A. In vivo fiber tractography using DT-MRI data. *Magn Reson Med* **44**, 625-632 (2000).
37. Paus, T. Growth of white matter in the adolescent brain: myelin or axon? *Brain Cogn* **72**, 26-35 (2010).
38. Beaulieu, C. The basis of anisotropic water diffusion in the nervous system - a technical review. *NMR Biomed* **15**, 435-455 (2002).
39. Tozer, D.*, et al.* Quantitative magnetization transfer mapping of bound protons in multiple sclerosis. *Magn Reson Med* **50**, 83-91 (2003).
40. Dula, A.N., Gochberg, D.F., Valentine, H.L., Valentine, W.M. & Does, M.D. Multiexponential T2, magnetization transfer, and quantitative histology in white matter tracts of rat spinal cord. *Magn Reson Med* **63**, 902-909 (2010).
41. Yarnykh, V.L. & Yuan, C. Cross-relaxation imaging reveals detailed anatomy of white matter fiber tracts in the human brain. *Neuroimage* **23**, 409-424 (2004).
42. Stikov, N.*, et al.* Bound pool fractions complement diffusion measures to describe white matter micro and macrostructure. *Neuroimage* **54**, 1112-1121 (2011).
43. Whittall, K.P.*, et al.* In vivo measurement of T2 distributions and water contents in normal human brain. *Magn Reson Med* **37**, 34-43 (1997).
44. Vavasour, I.M.*, et al.* Multi-parametric MR assessment of T(1) black holes in multiple sclerosis : evidence that myelin loss is not greater in hypointense versus isointense T(1) lesions. *J Neurol* **254**, 1653-1659 (2007).
45. Laule, C.*, et al.* Long T2 water in multiple sclerosis: what else can we learn from multi-echo T2 relaxation? *J Neurol* **254**, 1579-1587 (2007).
46. Volz, S., Noth, U. & Deichmann, R. Correction of systematic errors in quantitative proton density mapping. *Magn Reson Med* **68**, 74-85 (2012).